Available online at www.sciencedirect.com
SCIENCE DIRECT
ELSEVIER
International Journal of Mass Spectrometry 254 (2006) 202–209
International Journal of Mass Spectrometry
www.elsevier.com/locate/ijms

Formation, deposition and examination of size selected metal clusters on semiconductor surfaces: An experimental setup

Paul Kemper, Andrei Kolmakov, Xiao Tong, Yigal Lilach, Lauren Benz, Manuel Manard, Horia Metiu, Steven K. Buratto, Michael T. Bowers *

Department of Chemistry and Biochemistry, University of California, Santa Barbara, California 93106-9510, United States

Received 24 February 2006; received in revised form 26 May 2006; accepted 27 May 2006

Abstract

An instrument designed to investigate the chemical behavior of size selected metal clusters on semiconductor surfaces is described. The clusters are formed using laser vaporization, mass selected in a magnetic mass analyzer and deposited on TiO_2 substrates under UHV conditions with impact energies ranging from ≤1 to >100 eV/atom. Intensities of mass selected Au_n^+ and Ag_n^+ clusters range from 0.03 to 3 nA. Intensity, beam focusing and deposition energy are discussed. Once deposited on the surface, the clusters are investigated using scanning tunneling microscopy (STM) and/or temperature programmed desorption (TPD). Examples are presented showing STM images of Au_5 deposited on a clean rutile titania surface and of the TPD of propene from TiO_2.
© 2006 Elsevier B.V. All rights reserved.

Keywords: Catalysis; Size selected; Metal clusters; Ion source

1. Introduction

As part of a long ongoing effort to unravel the intricacies of metal particle catalysis, a large experimental effort has been undertaken in the last 15 years to examine directly the behavior of metal clusters on surfaces. These experiments are typically done under UHV conditions as a controlled first step toward understanding actual catalysis that occurs under much more complex conditions. And, because the effect of cluster size is fundamentally interesting and of probable catalytic importance, the effort has recently centered on size selected clusters. The experimental challenges are substantial. These experiments require: (1) an ion source capable of producing 100's to 1000's of pA of mono-dispersed clusters; (2) some means of size selecting the desired cluster; (3) a UHV deposition section where the ions can be landed on a well characterized surface (preferably at low energy); (4) the appropriate surface science instrumentation necessary to examine those aspects of the cluster behavior that are of interest. Different groups have taken different approaches in meeting these requirements, especially as to the cluster source design.

Heiz and co-workers [1–3] use a high frequency laser vaporization source followed by a quadrupole beam bender and quadrupole mass selector. The source (similar to that of Gangopadhyay and Lisy [4]) uses an eccentrically orbiting metal sample disk and produces ∼1 nA of Nb_n^+ ($n = 2$–20). Up to 8 nA of atomic Nb^+ could be produced. The mass selected clusters are deposited on semiconductor or metal surfaces which could be cooled to ∼100 K. Analysis probes include temperature programmed desorption (TPD), Fourier transform infrared spectroscopy (FTIR), X-ray and UV photoelectron spectroscopy (XPS/UPS). Neither scanning tunneling microscopy (STM) nor atomic force microscopy (AFM) is included. Very narrow kinetic energy distributions of the ion beam are observed (∼0.5 eV FWHM).

Anderson and co-workers [5,6] use laser vaporization and magnetron sputtering sources. Here, the sample is rastered under computer control. Ions exiting the source are transported by a phase space compressing quadrupole beam line through a quadrupole mass selector. Cluster ion KE distributions are narrow (<1 eV FWHM, for Ar^+ ions formed via electron impact). Ni_n^+ ($n = 2$–10) currents of ∼0.03–0.75 nA were produced at the

* Corresponding author. Tel.: +1 805 893 3049.
E-mail address: bowers@chem.ucsb.edu (M.T. Bowers).

1387-3806/$ – see front matter © 2006 Elsevier B.V. All rights reserved.
doi:10.1016/j.ijms.2006.05.020

target [7]. Analysis capabilities include TPD, XPS/UPS/Auger and low energy ion scattering spectroscopy (ISS).

Jödicke et al. [8] use a sputtering source in which high energy Kr^+ ions (produced in a cold reflex discharge ion source (CHORDIS)) are focused onto a metal target. Cluster ion currents of 0.1–1 nA of Ag_n^+ (n = 1–20) are produced with a 20 keV Kr^+ primary beam. The quadrupole mass selected beam can be deposited at temperatures down to ∼20 K and are examined with thermal energy atom scattering (TEAS) and STM (also cryogenic).

Palmer and co-workers [9,10] use a magnetron plasma sputtering source to produce clusters from 2 to >8000 Ag atoms (>60,000 Cu atoms). Much smaller clusters of Au and Si are formed. Mass selected intensities are in the range of 10's of pA. The selection is via a pulsed lateral time-of-flight (TOF) arrangement ($M/\Delta M$ is constant and ∼25) [11]. The deposited clusters are examined with room temperature STM. The ion kinetic energy spread is large with a FWHM in the range of 10's of eV.

Kaiser et al. [12] use a pulsed arc expansion source to produce antimony clusters from Sb_2^+ to Sb_{13}^+. No information is given as to intensity. Mass selection is done with a (rather clever) TOF/pulsed electrostatic mirror arrangement. Both scattering from, and deposition on, highly oriented pyrolitic graphite (HOPG) were done. The deposited clusters were examined with room temperature STM. The Meiwes-Broer group [13] also uses a pulsed arc discharge source to form clusters which are examined by STM. No mass selection is performed, however.

Klingeler et al. [14] make dosed fullerene clusters with a Smalley type laser vaporization source. The laser enters through the exit nozzle (as in the Lisy–Heiz source). A magnetic sector is used for cluster selection ($M/\Delta M \sim$ 1000–3000). Deposition is normally on HOPG and the clusters are studied with room temperature STM. Cluster currents on the order of 1 pA were reported. Deposition energies of ∼180 meV/atom for $Cs@C_{60}^+$ were used.

Binns and co-workers [15,16] use a continuous flow gas aggregation source (heated crucible in He) to produce nanometer sized clusters (200–600 atoms). A quadrupole with axial ionizer produces mass selected ionic clusters which are deposited on cooled metal substrates (40 K). Neutral clusters can be deposited directly without size selection. Ion currents are "considerably less" than laser vaporization sources. The KE spread in the dispersed clusters is large in absolute terms (∼50 eV FWHM) but small on a per atom basis (∼0.25 eV/atom).

In the design of Laaksonen et al. [17], the output from a pulsed laser vaporization disk source is quadrupole mass selected and then either deposited or further analyzed in a linear TOF. A quadrupole bending lens directs the beam. Currents of ∼5–10 pA (Si_{12}^+) were observed. The ion KE distribution was not discussed.

In the following sections, we first describe the design and, second, the performance of a new instrument for depositing mass selected metal clusters on semiconductor surfaces under UHV conditions. In our first experiments, room temperature STM and temperature controlled desorption are utilized to interrogate the system. An example of each will be given.

2. The instrument

In general terms, the present instrument consists of a pulsed laser vaporization source, a magnetic sector, an intermediate collector and finally, UHV chambers for deposition and STM imaging. The cluster ions move through five stages of differential pumping. An overview is shown in Fig. 1; the individual sections are discussed below.

2.1. Ion source

The laser vaporization ion source is shown in Fig. 2. The operating principles of these sources have been discussed elsewhere [18] and only the details relevant to the present design are presented here. The sample format is a rotating translating 2 mm × 50 mm rod. The rod is mounted vertically directly in the "waiting room" (∼1 cm^3), directly in front of the pulsed valve orifice (General Valve, Series 9). Ions exit through an expansion nozzle insert of variable bore and length (typically 1.5 mm × 20 mm). In contrast to other reports [1,4], we do not find that these dimensions greatly affect the cluster distribution or intensity. Argon is used as the expansion gas (rather than the more commonly used Helium) as it seems to result is significantly greater clustering. Neon and Krypton were also tried with no apparent improvement. The valve open time and the delay time between valve and laser are variable and are critical adjustments. The Ar backing pressure is not critical, perhaps because the valve open time is adjustable. The metal samples last about 8 h and are easily replaced (about 1–2 h from working experiment to working experiment).

The green line (532 nm) of a Nd-YAG laser (SpectraPhysics Lab Pro 290; 500 mJ/pulse, 50 ± 5 Hz.) is focused on the sample through the nozzle orifice. A 1500 mm focal length plano-convex single lens is used and gives a spot size of ∼0.4 mm. The available laser power is far greater than optimal and a polarization rotator/splitter cube combination is used to adjust the power incident on the sample. This is a critical adjustment.

The ion beam exits the source vacuum chamber through a 3 mm diameter skimmer (Beam Dynamics). The distance between nozzle exit and skimmer is adjustable (0–50 mm) which has a small effect on the cluster size distribution. A focusing lens is mounted between the nozzle orifice and skimmer and application of −10 to −20 V (with respect to the nozzle) on this lens has a substantial effect on the ion intensity (despite the high pressure in this region). The source/nozzle assembly is electrically biased (∼150 V) with respect to the skimmer (0 V). This is also a critical parameter. The total ion current out of the source is read on the skimmer and used for rough tuning of the source parameters.

The source chamber (Fig. 1) consists of a 6″ (tube diameter) five-way cross. The ion source assembly is mounted entirely on one ISO160 flange for ease of removal. Source alignment is maintained by four locating rods mounted on the skimmer flange which plug into the source assembly. The chamber is pumped with a helical grooved molecular pump (440 l/s, Osaka TS440) backed by a 44 m^3/h rotary pump (Edwards E2M40). This arrangement maintains a constant pumping speed up to

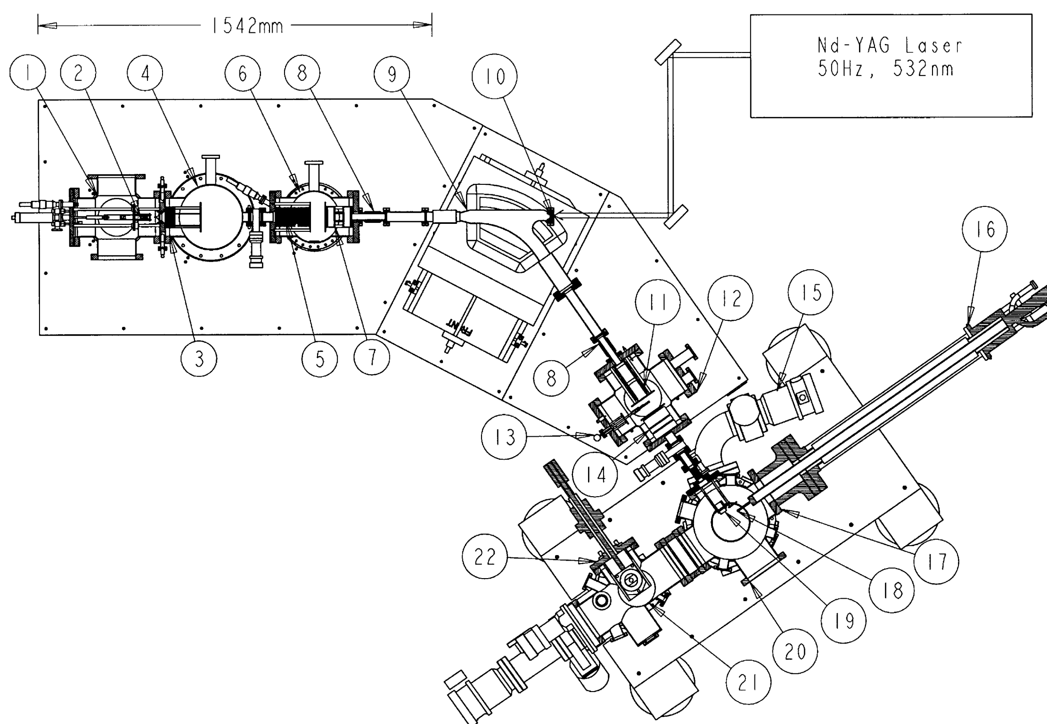

Fig. 1. Overall view of instrument (drawn to scale). The absolute dimension of the laser vaporization source and associated pumping/expansion region is indicated: (1) source chamber; (2) cluster source (see Fig. 2); (3) first einzel/steering lens; (4) diffusion pump chamber; (5) second einzel/steering lens; (6) acceleration chamber; (7) acceleration/focus lens (see Fig. 3); (8) ceramic break; (9) magnet flight tube; (10) laser entrance window; (11) deceleration/*y* focus lens; (12) deceleration/collector chamber; (13) moveable detector; (14) *z* focus/steering lens; (15) turbo pump; (16) cryo-manipulator; (17) deposition chamber; (18) sample holder stage; (19) final focus lens; (20) Auger; (21) microscope chamber; (22) microscope.

source chamber pressures of almost 10^{-2} Torr and can handle source chamber pressures in the Torr range. The base pressure in the chamber is in the low 10^{-7} Torr range.

2.2. First differential pumping section

We use four stages of differential pumping to maintain nine decades of pressure differential between the ion source and UHV deposition regions. The first comes directly after the skimmer and consists of a 10″ chamber pumped by a 2400 l/s diffusion pump (Edwards 250 M) backed by a 20 m^3/h rotary pump. The base pressure is $\sim 2 \times 10^{-9}$ Torr which rises to $\sim 2 \times 10^{-5}$ Torr during deposition. This chamber contains the first einzel/steering lens and ends with a 1.5″ gate valve. The valve allows the source to be removed without venting the rest of the instrument. A solid copper gasket with a 6 mm hole is used between the chamber and valve to provide additional pressure isolation when the valve is open. The laser and ion beams are far smaller than this diameter and no loss of intensity results.

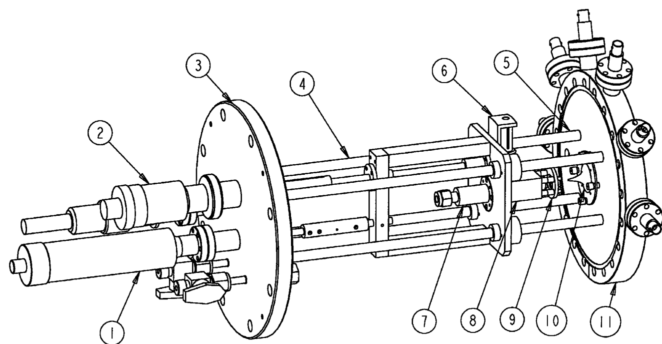

Fig. 2. Ion source: (1) sample drive rotary motion feed through; (2) source linear position feed through; (3) ISO160 source mounting flange (all source connections are made here); (4) source linear position guide rods; (5) source locating posts (on skimmer flange); (6) rotation/translation mechanism; (7) pulsed valve; (8) source body; (9) focusing lens; (10) skimmer; (11) skimmer flange.

2.3. Acceleration chamber

The next section consists of an 8″ chamber pumped by a 1100 l/s Turbo Pump (Osaka TG1133M) backed by a 20 m^3/h rotary pump. The chamber provides another level of pressure isolation with a base pressure of $\sim 1 \times 10^{-9}$ Torr ($\sim 1 \times 10^{-8}$ Torr during deposition). The chamber also contains a second einzel/steering lens and the acceleration slit/optics for the magnetic sector. Up to this point, the ion optics has cylindrical symmetry. However, because the magnetic sector has different *y* and *z* focusing properties, the acceleration lens must have a separate lens element for each dimension (Fig. 3).

The ions must be accelerated prior to entering the magnet. To avoid biasing the source (and sample substrate) at high voltage, the magnet flight tube is instead biased (800–1000 V typically). Ceramic breaks are used for isolation and the acceleration voltage is carried through the break on an internal tube. The sector

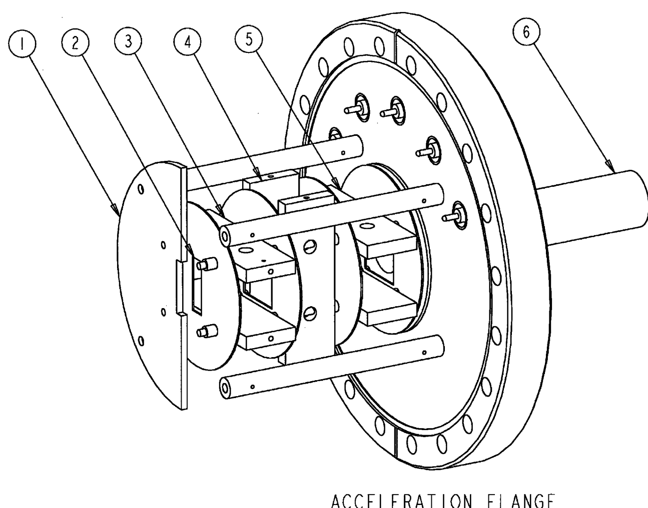

Fig. 3. Acceleration slit optics: (1) initial orifice (0 V, cut away to show acceleration slit); (2) acceleration slit; (3) z steering plates; (4) y focus plates; (5) z focus plates; (6) high voltage shield. The beam direction is in the x direction and a right-handed coordinate system defines the y- and z-directions.

was optimized for transmission rather than resolution and a 3 mm × 10 mm acceleration slit is used.

2.4. Magnetic sector

A magnetic sector was chosen as the dispersion element for several reasons. (1) Magnet sectors have high mass capability. At 1 kV accelerating potential, the mass range extends to ∼8000 amu. Even higher masses can be transmitted at lower voltages (with lower resolution). (2) First order spatial focusing. The accelerating slit is reimaged at the deceleration slit providing excellent transmission and ease of focusing. (3) The curved flight tube provides an obvious path for the laser beam down the ion beam axis (Fig. 1). Neutral clusters are also naturally rejected. The actual sector used has a 55° included angle and a radius of 298.5 mm. The flight tube is not separately pumped but functions as a differential pumping orifice due to its low conductance (8.5 mm × 50 mm cross section). As noted above, the flight tube is floated 800–1000 V above ground to provide the accelerating potential.

2.5. Deceleration and intermediate collector chamber

Following the magnetic sector, the ions enter the collector chamber. Here, they pass through the deceleration slit (3 mm × 10 mm) and a y focus/steering lens. At this point, they can be collected on a moveable disk and the ion current read on an electrometer (Keithly 6517A). Mass spectra and ion kinetic energy distributions are measured here. The KE distributions are measured by interposing a highly isolated, variable voltage source between the electrometer and the collector. Since the electrometer input is a virtual ground, the added potential measures the effective source voltage with respect to ground.

In order to deposit clusters on a sample substrate, the collector is moved out of the beam path. The ions then pass through a z focus/steering lens and on to the deposition chamber.

The collector chamber is a 6″ (tube dimension) five-way cross. It is pumped by a 430 l/s turbo pump (Osaka TG413M) backed by a 20 m^3/h rotary pump. The base and deposition pressures are both ∼1 × 10^{-9} Torr. The chamber ends with a 1.5″ gate valve which allows the UHV sections that follow to be isolated when deposition is not underway. A welded bellows/differentially pumped rotary coupling assembly is used to connect to the deposition chamber. This is necessary to allow for both rock and pitch of the UHV chambers on the air table (see below).

2.6. Deposition chamber

The next two sections (deposition and microscope chambers, respectively) constitute the UHV portion of the instrument. They are joined with a 6″ gate valve and ride together on an air flotation, vibration isolation table. Connection with the rest of the instrument (which is not floated) is through the flexible rotary coupling noted above. Samples are moved from chamber to chamber and held for deposition (and other UHV experiments) on a long-reach, four axis, cryogenic manipulator (VG Helitran 1000) which is temperature variable from ≤10 to 300 K.

The sample substrates (usually TiO_2) are mounted in a universal sample holder (OFHC copper; Fig. 4), which can be transferred from station to station (via the manipulator) and to the STM for imaging. Along with the substrate, the sample holder contains a silicon resistance heater and a thermocouple (TC) for sample temperature readout.

During deposition, the ion clusters enter the deposition chamber and pass immediately through a final focusing lens inside the chamber. The sample substrate is positioned directly behind this lens. The current on the sample is read in the same manner as described above (with the moveable detector) and the deposition energy varied with the same interposed voltage (now applied to the sample). The sample holder mount is electrically isolated but thermally connected to the cryo-manipulator via sapphire wash-

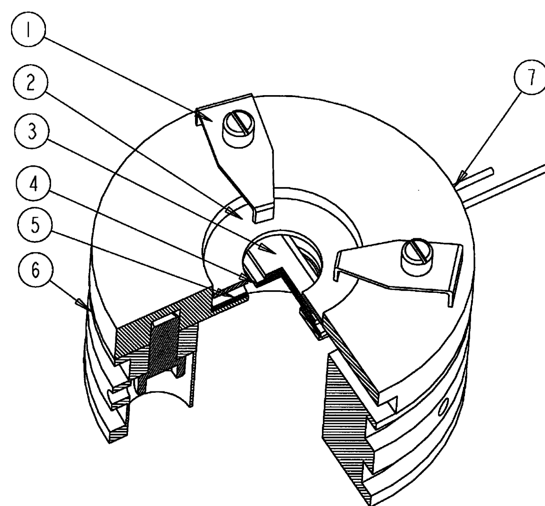

Fig. 4. Sample holder: (1) retainer clips; (2) sapphire washer; (3) sample substrate; (4) silicon heater; (5) sapphire washer; (6) sample holder body; (7) thermocouple connection.

ers. The manipulator can cool the sample holder to ∼10–20 K allowing low temperature deposition and ultra soft landing on an Argon or Krypton film.

The deposition chamber itself is a 12″ cylinder with three experimental tiers. It also houses the temperature programmed desorption (TPD) experiment and the XPS/Auger diagnostics (see below).

The chamber is pumped with a 500 l/s ion pump (Varian VacIon) together with a Ti sublimation pump and liquid N_2 baffle. A 285 l/s UHV rated turbo pump (Osaka TH261M) backed by a 36 m^3/h scroll pump (Edwards GVSP30) is used during pump down and bake out. The base pressure is below 1×10^{-10} Torr.

2.7. Microscope chamber

This final chamber contains the microscope unit as well as metal vapor deposition sources and the argon ion gun used to prepare the substrate surfaces. As noted, samples are moved into this chamber with the long-reach manipulator. There is a separate load lock/manipulator entrance to introduce new samples and microscope tips.

The microscope (RHK STM100/AFM100) has both STM and AFM capabilities. The sample stage (where the sample holder is mounted) can be cooled to ∼25 K to allow temperature dependent studies of cluster behavior. The microscope performance is discussed below, but one point is worth noting: the entire instrument is housed on the fourth floor and building vibration clearly occurs. Despite this, the standard air suspension vibration isolation table provides sufficient isolation for routine atomic resolution.

For largely historic reasons, sample preparation (Ar^+ bombarding and annealing) is done on the microscope stage. This is clearly not optimal since it entails back filling the chamber with Argon gas as well as flashing impurities off the sample. A separate preparation chamber is planned.

The chamber is pumped with a 300 l/s ion pump (Varian VacIon) together with a Ti sublimation pump and liquid N_2 baffle. The base pressure is $\sim 5 \times 10^{-11}$ Torr. A second, UHV rated turbo pump (Osaka TH261M) is used during pump down and bake out. It is also used to evacuate the load lock.

2.8. General features

Bake out in the ion source through collector chambers is with internal quartz-halogen lamps. Heating tapes and band heaters are used on the UHV chambers and the magnet flight tube. Bake out of the microscope is limited to 120 °C. Either positively

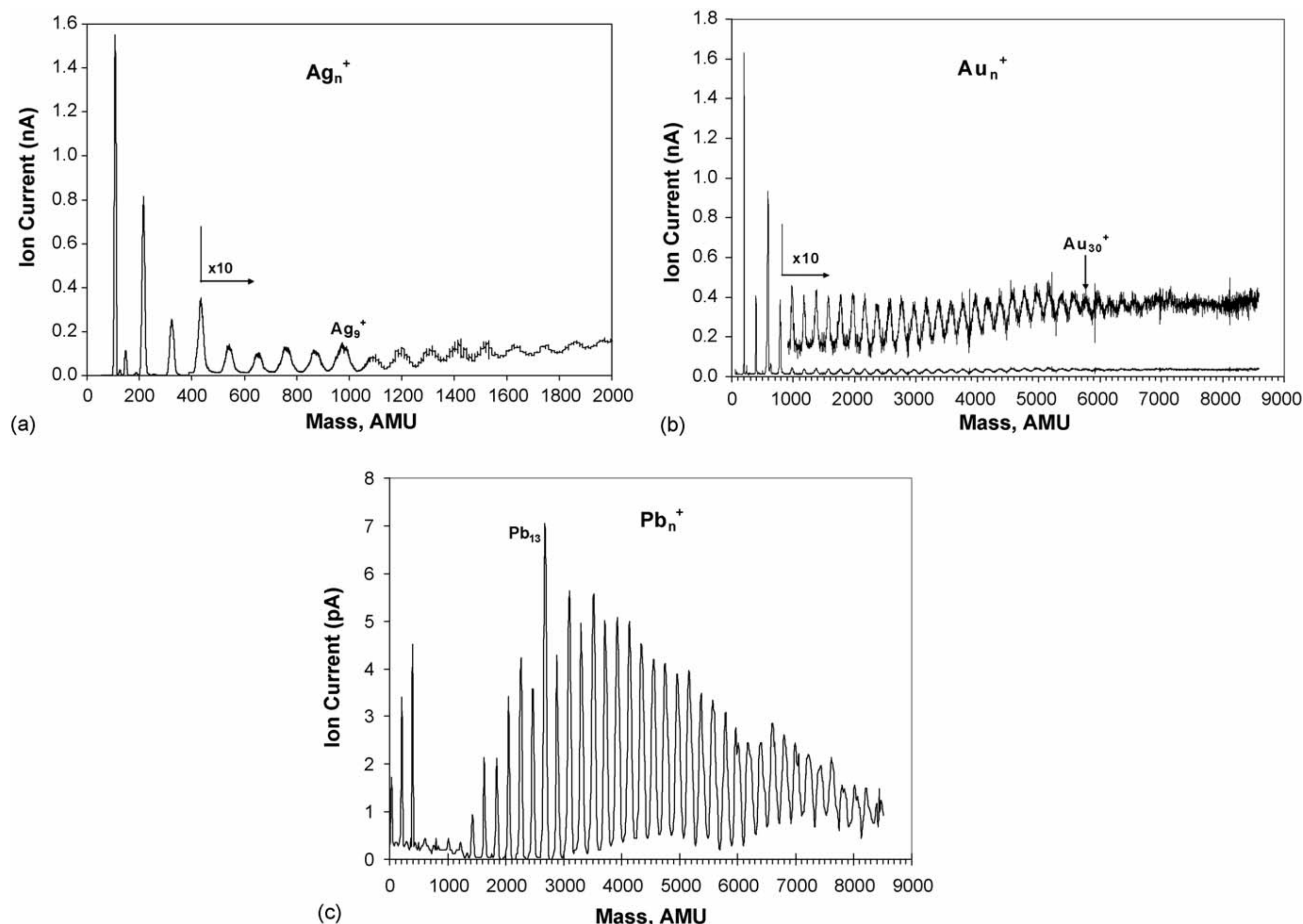

Fig. 5. (a) Ag_n^+ mass spectrum, 0–2000 amu; (b) Au_n^+ mass spectrum, 0–8500 amu; (c) Pb_n^+ mass spectrum, 0–8500 amu. Note the resolution and bimodal intensity distribution.

or negatively charged clusters can be deposited. To date, the positive clusters have been more intense.

3. Instrument performance

3.1. Cluster source

3.1.1. Intensity and resolution

Fig. 5a shows a typical mass scan of silver clusters Ag_n^+ ($n = 1$–16). Intensities range from 1.5 nA to ∼20 pA (Ag_{16}^+). The source tuning here is a compromise between high and low atom numbers, and Ag^+ and Ag_2^+ currents an order of magnitude larger can be produced. The peak at 150 amu is $AgAr^+$. Fig. 5b shows an extended mass scan of gold clusters from 0 to 8500 amu. Intensities for $Au_{1–4}^+$ range from 0.4 to 1.6 nA while those for $Au_{5–40}^+$ are roughly 30 pA. Fig. 5c shows a similar scan of Pb_n^+ clusters with better resolution. From this scan, the mass resolution ($M/\Delta M$) is seen to be ≥40 at 8500 amu, allowing selection of individual clusters up to Au_{40}. The low mass/high mass, bimodal intensity distribution seen in Fig. 5c is seen with Ag_n^+ as well. It would seem to indicate that clustering is too efficient in the present source; however, attempts to "push" the ion intensity at high atom numbers to smaller sizes have not yet been successful.

The present cluster intensities of 0.1–1 nA for Ag_n^+ and Au_n^+ correspond to deposition times of ∼10–100 min (for ∼0.02 ML) and are adequate.

3.1.2. Ion kinetic energy distribution

In the absence of collisions, the cluster ion deposition energy is given by the difference between source and substrate potentials. When gas is present, energy is added in the expansion and subtracted by collisions in the acceleration region between the nozzle and skimmer. The velocity added in the expansion is fairly uniform while a Poisson's distribution of collision numbers (ranging from 0 to several) governs the energy lost. The expected result is a KE distribution with some fraction of clusters having a uniform maximal energy equal to the acceleration potential (i.e., source to ground potential, ∼150–200 eV) with the energies of the remainder of the ions tailing off to lower values. This is in fact what is found. Fig. 6a shows a plot of Ag^+ ion current versus detector stopping potential for an acceleration

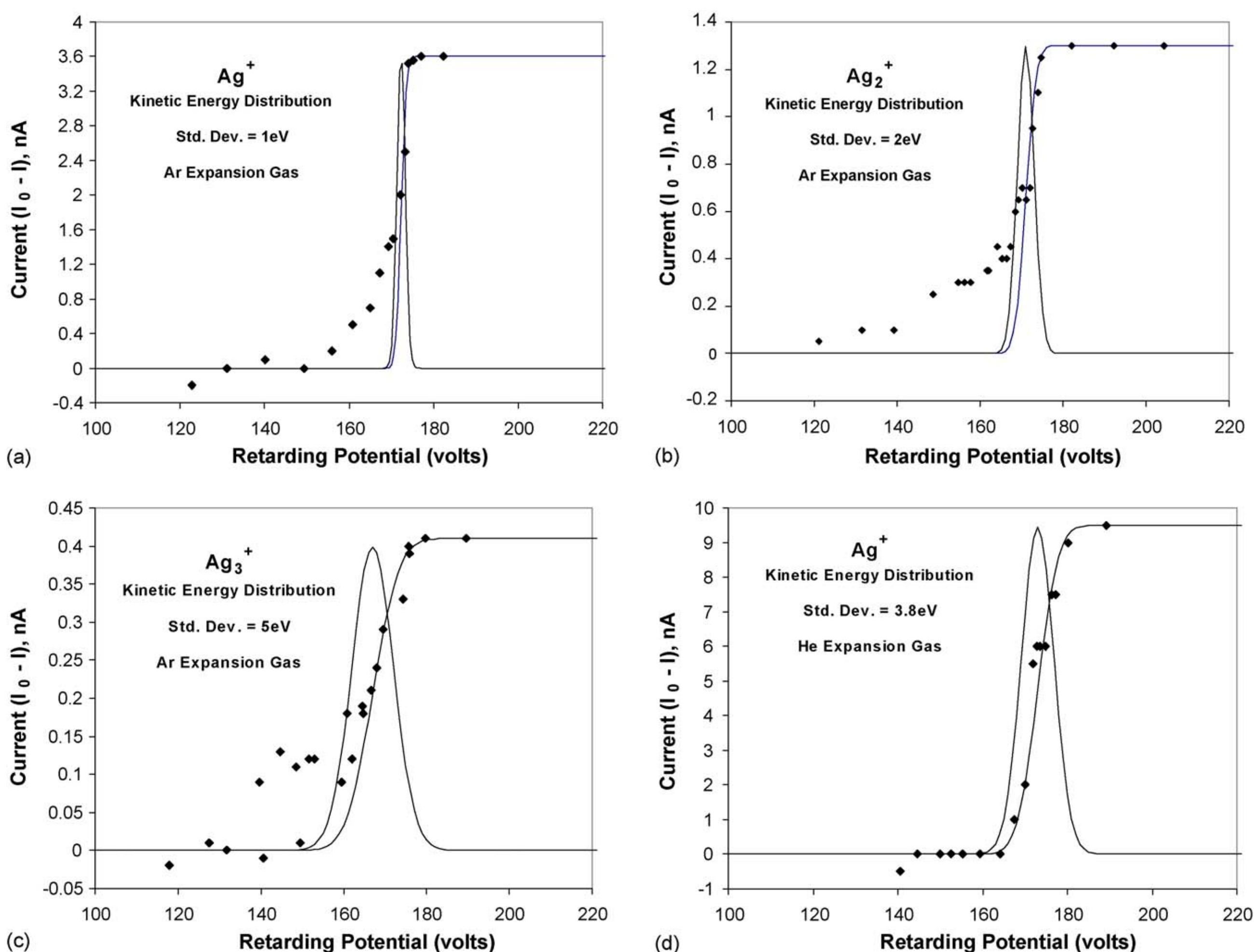

Fig. 6. (a) Kinetic energy distribution of Ag^+ at the collector. With a deceleration potential of 167 V, about 50% of the ions are collected and have a KE range of about 0–4 eV. (b) Ag_2^+ KE distribution. Similar results with a range of deposition energies from 0 to 5 eV. (c) Ag_3^+ KE distribution. Similar results with a range from ∼0 to 9 eV. (d) Same as (a) except with He as the expansion gas. Note the lack of tailing to low energy. The range of deposition energies here is from 0 to 7 eV.

potential of ∼180 V. Superimposed on the data is an integrated normal distribution (fit to the high energy side of the data) as well as its derivative. Note that the high energy half of the distribution is quite sharp (∼1–2 eV wide) with an energy corresponding to the source acceleration potential. This narrow distribution is critical because it is the high energy side of the distribution which is deposited after retardation to 50% ion loss. The low energy part of the distribution – although broad – is lost when the cluster ions are decelerated before deposition. We can thus deposit ions with <2–3 eV/cluster. The KE range does increase with cluster size (Fig. 6b and c) but the maximum KE/atom is roughly constant.

Fig. 6d shows the result when He is used as an expansion gas. The low energy tail essentially disappears, presumably because of the much lower energy Ag^{+}/He collisions. The overall width of the distribution is wider than that found with Ar, however. The reason for this is unclear.

The degree of tailing does depend on the expansion gas pressure and at high enough pressures the low energy tail could theoretically overtake the entire distribution. Under actual experimental conditions, however, about 50% of the ions fall in the narrow, high energy part of the distribution.

3.1.3. Ion beam focusing

The size of the ion beam as it is focused on the sample directly affects the deposition time. In the present experiment, this size was measured by simply moving a small target through the beam and found to be ∼4 mm diameter after deceleration. No masks are used. The focusing for minimal size at the sample has not been fully optimized due to problems with electrical isolation between the sample and sample holder and we anticipate being able to reduce this spot size further. Although the beam density has not been characterized in detail, from STM observations we find the cluster density to be fairly uniform across the surface.

3.2. TPD experiments

Temperature programmed desorption experiments are carried out in the deposition chamber using a quadrupole mass spectrometer (Stanford Research Systems RGA200). During these experiments, the sample sits in a custom designed fork on the end of the cryogenic manipulator, positioned ∼1 mm below a 3 mm diameter orifice nose cone which covers the mass spectrometer filament. The titania sample (Princeton Scientific Corp.) is 1 cm in diameter, and is electrically isolated from the sample holder with sapphire washers. A K-type thermocouple is pressed between backside of the sample and a sapphire window. Below this window is a doped silicon wafer, which can be resistively heated to temperatures >1300 K. Fig. 7 shows an example TPD spectra (mass 41, 1 K/s) taken of propylene exposed at 110 K on clean titania. The peak at ∼200 K matches well with previous TPD studies by Ajo et al. [19]. Exposures reported here have not been corrected for doser enhancement or ion gauge sensitivity, and are therefore only accurate to within a factor of two (at best). The low temperature peak at ∼125 K which emerges at higher exposures is likely due to multilayer formation. TPD experiments on surfaces decorated with size-selected Au clusters will be published elsewhere.

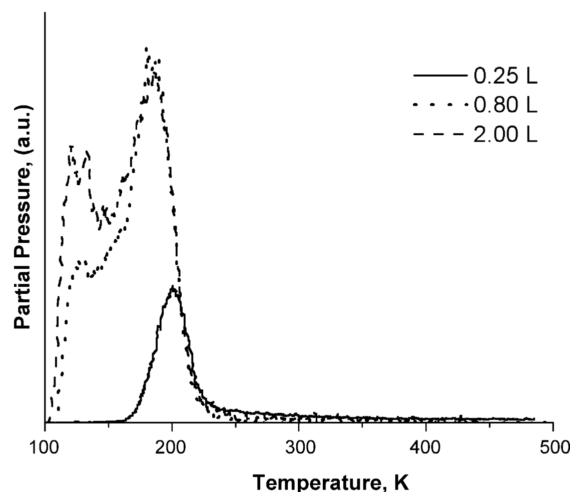

Fig. 7. Temperature programmed desorption spectra of propylene, adsorbed at 100 K, from a reduced titania surface.

3.3. STM experiments

We use STM to examine the titania surface prior to and following the deposition of mass-selected clusters. Fig. 8a shows a clean image of the titania surface (85 Å × 85 Å), in which bright rows correspond to titanium atoms, and dark rows to oxygen

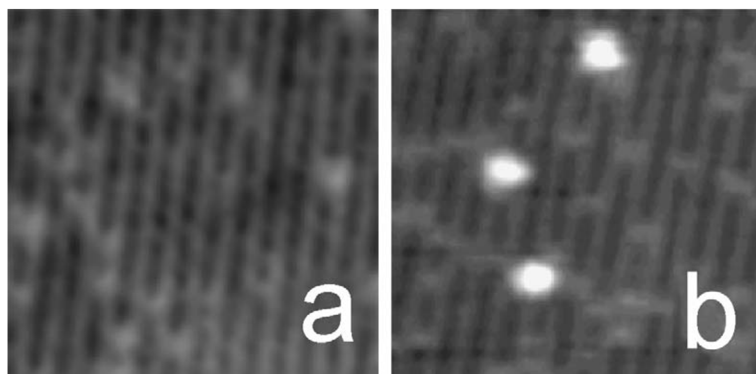

Fig. 8. STM images of: (a) a clean rutile titania (1 1 0)-(1 × 1) surface and (b) a titania surface following the deposition of mass-selected Au_5 clusters. Both images are 85 Å × 85 Å.

atoms [20]. Bright features visible between titanium atom rows correspond to oxygen atom vacancies [20]. A tunneling current of 0.1–0.2 nA is typical, with a sample bias of +1 to +2 V. Fig. 8b shows the surface following the deposition of Au_5^+, in which three bright features are observed, which we assign as intact Au_5 clusters on the surface [21]. Information can be extracted from such images about the size, shape, adsorption site and mobility of mass-selected clusters as shown elsewhere [22–26].

Acknowledgements

The authors wish to acknowledge the support of the Air Force Office of Scientific Research under DURINT Grant F49620-01-04J9. We would also like to thank Dr. J. Schmidt for help in the assembly of the instrument.

References

[1] U. Heiz, F. Vanolli, L. Trento, W.-D. Schneider, Rev. Sci. Instrum. 68 (1997) 1986.
[2] K. Judai, A.S. Wörz, S. Abbet, J.-M. Antonietti, U. Heiz, A. Del Vitto, L. Giordano, G. Paccioni, Phys. Chem. Chem. Phys. 7 (2005) 955.
[3] S. Abbet, K. Judai, L. Klinger, U. Heiz, Pure Appl. Chem. 74 (2002) 1527.
[4] P. Gangopadhyay, J.M. Lisy, Rev. Sci. Instrum. 62 (1991) 502.
[5] K.J. Boyd, A. Łapicki, M. Aizawa, S.L. Anderson, Rev. Sci. Instrum. 69 (1998) 4106.
[6] K.J. Boyd, A. Łapicki, M. Aizawa, S.L. Anderson, Nucl. Instrum. Methods Phys. Res. B 157 (1999) 144.
[7] M. Aizawa, S. Lee, S.L. Anderson, J. Chem. Phys. 117 (2002) 5001.
[8] H. Jödicke, R. Schaub, A. Bhowmick, R. Monot, J. Buttet, W. Harbich, Rev. Sci. Instrum. 71 (2000) 2818.
[9] S. Pratontep, S.J. Carroll, C. Xirouchake, M. Streun, R.E. Palmer, Rev. Sci. Instrum. 76 (2005) (Art. no. 045103).
[10] R.E. Palmer, S. Pratontep, H.G. Boyen, Nat. Mater. 2 (2003) 443.
[11] B. vonIssendorff, R.E. Palmer, Rev. Sci. Instrum. 70 (1999) 4497.
[12] B. Kaiser, T.M. Bernhardt, K. Rademann, Nucl. Instrum. Methods Phys. Res. B 125 (1997) 223.
[13] G. Ganteför, H.R. Siekmann, H.O. Lutz, K.H. Meiwes-Broer, Chem. Phys. Lett. 165 (1990) 293.
[14] R. Klingeler, P.S. Bechthold, M. Neeb, W. Eberhardt, Rev. Sci. Instrum. 73 (2002) 1803.
[15] S.H. Baker, S.C. Thornton, K.W. Edmonds, M.J. Maher, C. Noris, C. Binns, Rev. Sci. Instrum. 71 (2000) 3178.
[16] C. Binns, Surf. Sci. Rep. 44 (2001) 1.
[17] R.T. Laaksonen, D.A. Goetsch, D.W. Owens, D.M. Poirier, F. Stepniak, J.H. Weaver, Rev. Sci. Instrum. 65 (1994) 2267.
[18] (a) R.E. Smalley, Laser Chem. 2 (1983) 167, and references therein;
(b) S. Maruyamam, L.R. Anderson, L.R. Smalley, Rev. Sci. Instrum. 61 (1990) 3686;
(c) D.M. Cox, K.C. Reichmann, D.J. Trevor, A. Kaldor, J. Chem. Phys. 88 (1988) 111;
(d) P. Milani, W.A. deHeer, Rev. Sci. Instrum. 61 (1990) 1835;
(e) R.T. Laaksonen, D.A. Goetsch, D.W. Owens, D.M. Poirier, F. Stepniak, J.H. Weaver, Rev. Sci. Instrum. 65 (1994) 2267;
(f) J.F. Ready, Effects of High-Power Laser Radiation, Academic, New York, 1971.
[19] H.M. Ajo, V.A. Bondzie, C.T. Campbell, Catal. Lett. 78 (2002) 359.
[20] U. Diebold, J.F. Anderson, K. Ng, D. Vanderbilt, Phys. Rev. Lett. 77 (1996) 1322.
[21] X. Tong, L. Benz, P. Kemper, H. Metiu, M.T. Bowers, S.K. Buratto, J. Am. Chem. Soc. 39 (2005) 13516.
[22] X. Tong, L. Benz, A. Kolmakov, S. Chrétien, H. Metiu, S.K. Buratto, Surf. Sci. 575 (2005) 60.
[23] L. Benz, X. Tong, P. Kemper, Y. Lilach, A. Kolmakov, H. Metiu, M.T. Bowers, S.K. Buratto, J. Chem. Phys. 122 (2005) 081102.
[24] X. Tong, L. Benz, S. Chrétien, P. Kemper, A. Kolmakov, H. Metiu, M.T. Bowers, S.K. Buratto, J. Chem. Phys. 123 (2005) 204701.
[25] X. Tong, L. Benz, P. Kemper, H. Metiu, M.T. Bowers, S.K. Buratto, J. Am. Chem. Soc. 127 (2005) 13516.
[26] L. Benz, X. Tong, P. Kemper, H. Metiu, M.T. Bowers, S.K. Buratto, J. Phys. Chem. B 110 (2006) 663.